1 *Article*

Analysis of wide-lane ambiguities derived from geometry-free and geometry-based PPP model and their implication on orbit and clock quality

5 **Gang Chen [1], Sijing Liu [2,1,*] and Qile Zhao [3,*]**

6 [1] China University of Geosciences, College of Maritime Science and Technology, Wuhan, 430074, China;
7 ddwhcg@cug.edu.cn
8 [2] China University of Geosciences, Institute of Geophysics and Geomatics, Wuhan 430074, China;
9 sijingliu@cug.edu.cn
10 [3] Wuhan University, GNSS Research Center, Wuhan 430079, China; zhaoql@whu.edu.cn
11 * Correspondence: sijingliu@cug.edu.cn; zhaoql@whu.edu.cn; Tel.: +0086-0270-15629083635

13 **Abstract:** Orbit and clock products are used in real-time GNSS precise point positioning without
14 knowing their quality. This study develops a new approach to detect orbit and clock errors through
15 comparing geometry-free and geometry-based wide-lane ambiguities in PPP model. The
16 reparameterization and estimation procedures of the geometry-free and geometry-based
17 ambiguities are described in detail. The effects of orbit and clock errors on ambiguities are given in
18 analytical expressions. The numerical similarity and differences of geometry-free and geometry-
19 based wide-lane ambiguities are analyzed using different orbit and clock products. Furthermore,
20 two types of typical errors in orbit and clock are simulated and their effects on wide-lane
21 ambiguities are numerically produced and analyzed. The contribution discloses that the geometry-
22 free and geometry-based wide-lane ambiguities are equivalent in terms of their formal errors.
23 Although they are very close in terms of their estimates when the used orbit and clock for geometry-
24 based ambiguities are precise enough, they are not the same, in particular, in the case that the used
25 orbit and clock, as a combination, contain significant errors. It is discovered that the discrepancies
26 of geometry-free and geometry-based wide-lane ambiguities are coincided with the actual time-
27 variant errors in the used orbit and clock at the line-of-sight direction. This provides a quality index
28 for real-time users to detect the errors in real-time orbit and clock products, which potentially
29 improves the accuracy of positioning.

30 **Keywords:** Geometry-free; geometry-based; wide-lane ambiguity; orbit and clock residual error

31

1. Introduction

33 Precise point positioning (PPP) using global navigation satellite systems measurements (GNSS)
34 was initially proposed in [1] in order to solve the high computation burden of the network approach.
35 The PPP technique employs only a single receiver to determine its position without explicitly using
36 reference stations. To do so, precise orbit and clock are needed to enable absolute positioning of high
37 accuracy [2]. This technique has been intensively developed from static to kinematic positioning [3],
38 from post-processing to real-time service [4-5], from using GPS only to using multi-constellation
39 systems [6], from ambiguity-float to integer ambiguity-fixed solution [7-10], from decimeter to
40 centimeter accuracy [11]. The PPP technique has been started with the ionosphere-free combination
41 approach [1] and then developed with the raw observation approach [11-15]. One of the major
42 differences of these two approaches is that one eliminates the ionosphere delay while the other
43 estimates it. Another main difference is that how to deal with the ambiguity parameter. The
44 ambiguity term estimated with the ionosphere-free approach is actually a combination of narrow-

45 lane (NL) and wide-lane (WL) ambiguity, while the raw observation approach produces L1 and L2
46 ambiguity parameters simultaneously together with the ionosphere term (let us consider only the
47 case of dual frequencies). The common point for these two approaches is that their ambiguity
48 parameters do not have integer nature, as double-difference cannot be formed using a single receiver.
49 In this case, the satellite hardware delay cannot be separated or eliminated from the ambiguities in
50 the PPP mode. The term takes typically several tens of minutes to converge when the positioning
51 starts or resets after data interruption. The accuracy can be improved, and the convergence time can
52 be shortened if the ambiguities can be fixed correctly to their integers using additional corrections,
53 such as satellite phase biases.
54   A key task for the PPP integer ambiguity resolution is to separate or identify satellite phase
55 biases in the ambiguity term in the reference network and then to apply these biases to their
56 corresponding ambiguities in mobiles to restore integer nature [13-14]. The ionosphere-free approach
57 basically uses two parallel processes [7-10]. One process is to compute the geometry-free (GF) Hatch-
58 Melbourne-Wübbena combinations [16-18] in order to produce WL satellite phase biases and
59 integers. The other process is to carry out the geometry-based (GB) positioning to compute the
60 ionosphere-free ambiguity terms and further separate NL biases with involvement of integers of GF
61 WL ambiguities. The raw observation approach uses only one process that produces L1 and L2
62 ambiguities simultaneously [14], which are then used to form GB WL ambiguities and further
63 produce WL satellite phase biases. A variant of the raw observation approach is to produce WL and
64 L2 ambiguities simultaneously in the GB model [15]. WL ambiguities are the basis of going forwards
65 for these two approaches. The difference is that one produces them with the GF model while the other
66 with the GB model. Then the question raises: are the GF WL ambiguities the same or equivalent with
67 the GB ones from even a single receiver in terms of estimates themselves and their formal precision?
68 The reason for such a question is to clear off the hesitation of mixing use of the corrections. That is to
69 say, if they are not the same or equivalent, one may hesitate to apply the GB WL corrections to the
70 ionosphere-free approach, or apply the GF WL corrections to the raw observation approach in user
71 side. The question has been positively answered in an analytical way in [19] using a between-satellite
72 single-difference functional model of multiple stations. However, there is no numerical analysis
73 based on the real data in literature. It concludes that the GF WL ambiguity precision does not differ
74 too much from its GB counterpart under an assumption of small to regional networks [19]. This
75 assumption does not consider the orbit and clock residual errors (i.e. the remaining error in precise
76 orbits and clocks as they are not perfect). Different questions may then raise. Do the orbit and clock
77 residual errors make differences for the GF and GB ambiguities? This is certainly not the case for the
78 GF ambiguities as the geometry related parameters, such as satellite/receiver positions,
79 satellite/receiver clock as well as troposphere delay, are eliminated. Then how about the GB
80 ambiguities? If so, in what level of orbit and clock quality, one could claim that the GF and GB
81 ambiguities are equivalent?
82   The quality of orbit and clock has been improved in the past years for post-processing products
83 [20] and real-time products [21]. The majority of GNSS community is producing real-time orbit and
84 clock step by step [5-6]. A set of satellite orbit parameters (initial state and solar radiation pressure)
85 is first determined using a network of globally distributed reference stations using the past 24 - 48
86 hours of GNSS measurements. The orbits of at least 3 hours are predicted using the obtained orbit
87 parameters. The predicted orbits are then used as input for clock bias filtering in which real-time
88 observations are used. The accuracy of the predicted orbit is dominated by the solar radiation
89 pressure [6]. In addition, the predicted orbit may not be precise enough in the eclipse and just out of
90 the eclipse seasons, due to the fact that the yaw attitude is not properly modelled. It is obvious that
91 the remaining error of predicted orbits with longer predict arc length could make significant negative
92 impact on the GB NL ambiguity estimation and integer resolutions [6]. Their impact on GB WL
93 ambiguities remains being not analyzed. Although it is possible to reduce the orbit error by
94 shortening the predict length, the variation of errors could be a couple of centimeters to decimeters.
95 There are also exceptional occasions that some satellites, like GPS IIF, could have large errors up to
96 meters in their predicted orbits [22]. These errors could significantly worsen the clock bias estimation

97 and satellite phase bias estimation as well as PPP integer ambiguity resolution in user side, in
98 particular for real-time users.

99   It is common to evaluate the quality of real-time orbit and clock by comparing them with the
100 post-processing counterpart separately [21]. However, the post-processing products are available
101 only after one day or a couple of hours later, which is not very acceptable for real-time users. In
102 addition, it is well known that the clock products absorb partly the errors of predicted orbits,
103 particularly errors of the line-of-sight (LOS) direction [23-25]. Therefore, it is more reasonable to
104 assess orbit and clock residual error as a whole directly from a user's perspective. The differences
105 between GF and GB wide-lane ambiguities is a starting point to investigate.

106   This contribution aims at analysis of single-site ambiguities derived from both GF and GB
107 model. We focus on numerical computation and analysis using raw observations without differential
108 and combination operator in the measurement domain. The GB WL ambiguities are derived using
109 different orbit and clock products. To simplify the presentation and discussion, we are focusing on
110 global positioning system (GPS) in this contribution, but this does not affect the generality of our
111 analysis for other constellations. We also investigate the discrepancies between GF and GB WL
112 ambiguities to disclose the orbit and clock quality from a user's perspective. The contribution is
113 arranged as follows: First, the GF and GB models are respectively presented in detail. Second, the
114 effects of orbit and clock errors on the ambiguities are given in an analytical way. Third, the results
115 of GB and GF ambiguities are numerically analyzed for both post-processing and real-time orbit and
116 clock products. In addition, we simulate two types of errors in orbit and clock and reprocess the data
117 and investigate the impact on WL ambiguities for further understanding. Finally, the study is
118 summarized with some conclusions.

2. WL ambiguities derived from the GF model

120   The observation equation for measurements of code p and phase φ tracked by a receiver at
121 location r from GPS satellites s $(s = 1, 2, \cdots, n)$, at frequency i $(i = 1, 2)$ at epoch k, can be
122 expressed in meters as follows [26]:

$$E\{p^s_{i,r}(k)\} = \rho^s_r(k) + m^s_r \cdot T_r + \delta t_r(k) - \delta t^s(k) + \mu_i I^s_r(k) + d_{p_i,r} - d^s_{p_i}$$

$$E\{\varphi^s_{i,r}(k)\} = \rho^s_r(k) + m^s_r \cdot T_r + \delta t_r(k) - \delta t^s(k) - \mu_i I^s_r(k) + d_{\varphi_i,r} - d^s_{\varphi_i} + \lambda_i N^s_{i,r} \tag{1}$$

123 where $E\{\cdot\}$ denotes the expectation operator; $\rho^s_r(k)$ is the geometric range between the receiver
124 and satellite; T_r the zenith tropospheric delay with mapping function m^s_r; $\delta t_r(k)$ and $\delta t^s(k)$ the
125 receiver and satellite clock bias in meters, respectively; $\mu_i = \lambda_i^2 / \lambda_1^2$, λ_i the carrier wavelength of
126 frequency i; $I^s_r(k)$ the ionospheric delay; $d_{p_i,r}$ and $d_{\varphi_i,r}$ are the receiver hardware delays (or biases)
127 on code and phase, respectively; $d^s_{p_i}$ and $d^s_{\varphi_i}$ are the satellite hardware delays (or biases) on code and
128 phase, respectively; where it is assumed that these satellite hardware delays are relatively stable in
129 time; $N^s_{i,r}$ the integer carrier ambiguity. All terms with (k) are supposed to be significantly changed
130 in time.

131   The so-called GF observation model dispenses with geometric a priori information. The
132 geometry part is obtained by combining all non-dispersive terms, including the geometric range
133 $\rho^s_r(k)$, satellite $\delta t^s(k)$ and receiver clock $\delta t_r(k)$ and tropospheric delay $m^s_r \cdot T_r$. Even though, the
134 system is rank deficient. Not all terms are estimable. The hardware delays here are chosen as S-basis,
135 absorbed by other terms [19] . Let us define the geometry part as one common term for all
136 observations from one satellite:

$$R^s_r(k) := \rho^s_r(k) + m^s_r \cdot T_r + \delta t_r(k) - \delta t^s(k) + \frac{\mu_2}{\mu_2 - \mu_1}(d_{p_1,r} - d^s_{p_1}) - \frac{\mu_1}{\mu_2 - \mu_1}(d_{p_2,r} - d^s_{p_2}) \tag{2}$$

137   and the ionosphere term is also combined with part of satellite and receiver hardware biases:

$$\widetilde{I}_r^s(k) := I_r^s(k) + \frac{\mu_1}{\mu_2 - \mu_1}(d_{p_2,r} - d_{p_2}^s - d_{p_1,r} + d_{p_1}^s), \tag{3}$$

138   and the *ambiguity* terms for L1 and L2 frequency are defined as:

$$\widetilde{N}_{i,r}^s := N_{i,r}^s + \frac{1}{\lambda_i}\left\{ d_{\varphi_i,r} - d_{\varphi_i}^s + \frac{\mu_i + \mu_1}{\mu_2 - \mu_1}(d_{p_2,r} - d_{p_2}^s) - \frac{\mu_i + \mu_2}{\mu_2 - \mu_1}(d_{p_1,r} - d_{p_1}^s) \right\}, \tag{4}$$

139   Therefore, the *functional GF model* is written as

$$E\{p_{i,r}^s(k)\} = R_r^s(k) + \mu_i \widetilde{I}_r^s(k)$$
$$E\{\phi_{i,r}^s(k)\} = R_r^s(k) - \mu_i \widetilde{I}_r^s(k) + \lambda_i \widetilde{N}_{i,r}^s{}' \tag{5}$$

140   where the model is for a single satellite. Similar expressions can be seen in [19,27] with the single-
141   difference operator between satellites. Here, we focus on using raw measurements without any
142   difference and combination operator in observation domain. The epoch-wise solution of the
143   ambiguity term is simply computed as follows:

$$\mathbf{x}_k^s = \mathbf{H}\ \mathbf{z}_k^s, \tag{6}$$

144   where the phase and code measurements can be written in a vector form as
145    $\mathbf{z}_k^s := \begin{bmatrix} p_{1,r}^s(k) & p_{2,r}^s(k) & \phi_{1,r}^s(k) & \phi_{2,r}^s(k) \end{bmatrix}^T$ and the parameters that we are interested is ambiguity term
146    $\mathbf{x}_k^s := \begin{bmatrix} \widetilde{N}_{1,r}^s & \widetilde{N}_{2,r}^s \end{bmatrix}^T$. $\mathbf{H}$ is the coefficient matrix derived from Equation (5) only for ambiguity parameters
147   as follows:

148

$$\mathbf{H} := \begin{bmatrix} -\dfrac{1}{\lambda_1}\dfrac{\mu_2 + \mu_1}{\mu_2 - \mu_1} & \dfrac{1}{\lambda_1}\dfrac{2\mu_1}{\mu_2 - \mu_1} & \dfrac{1}{\lambda_1} & 0 \\[2ex] -\dfrac{1}{\lambda_2}\dfrac{2\mu_2}{\mu_2 - \mu_1} & \dfrac{1}{\lambda_2}\dfrac{\mu_2 + \mu_1}{\mu_2 - \mu_1} & 0 & \dfrac{1}{\lambda_2} \end{bmatrix}$$

149   The ionosphere and geometry terms are eliminated, which is the origin that the term of GF actually
150   comes from.
151   The stochastic model for the observation is given as follows:

$$\mathbf{Q}_{\mathbf{z}_k^s} = diag\{\sigma(e^s)_p^2, \sigma(e^s)_p^2, \sigma(e^s)_\phi^2, \sigma(e^s)_\phi^2\}, \tag{7}$$

152   where e^s is the elevation of the satellite. According to the *error propagation law*, the variance-covariance
153   of ambiguity terms can be derived as:

$$\mathbf{Q}_{\mathbf{x}_k^s} = \mathbf{H}\mathbf{Q}_{\mathbf{z}_k^s}\mathbf{H}^T, \tag{8}$$

154   where Equations (6) and (8) are used to compute the epoch-wise L1 and L2 ambiguities and their
155   variance-covariance. However, the epoch-wise observational model has no redundancy. The solution
156   is rather noisy as it is purely dominated by noise of code measurements. To increase the accuracy, an
157   averaging filter is implemented using multi-epoch solutions in a recursive way. Let us notate the
158   averaging solution as follows:

$$\hat{\mathbf{x}}_k^s := \begin{bmatrix} \hat{\widetilde{N}}_{1,r}^s & \hat{\widetilde{N}}_{2,r}^s \end{bmatrix}^T, \tag{9}$$

159   and the averaging filter starts at epoch 1 as $\hat{\mathbf{x}}_1^s = \mathbf{x}_1^s$ and $\mathbf{Q}_{\hat{\mathbf{x}}_1^s} = \mathbf{Q}_{\mathbf{x}_1^s}$.

160   Assume that the filtering solution at the epoch k-1 is denoted as $\hat{\mathbf{x}}_{k-1}^s$ with its covariance matrix
161    $\mathbf{Q}_{\hat{\mathbf{x}}_{k-1}^s}$, the variance-covariance is first updated with the assumed process noise for epoch solution at
162   k:

$$\mathbf{Q}_{\hat{\mathbf{x}}_{k,k-1}^s} = \mathbf{Q}_{\hat{\mathbf{x}}_{k-1}^s} + \mathbf{Q}_{\mathbf{w}}, \tag{10}$$

163 where, $\mathbf{Q}_{\mathbf{w}}$ is computed from the assumed process noise multiplying with time interval between
164 epoch k and k-1, and then updated with the epoch-wise variance-covariance

$$\mathbf{Q}_{\hat{\mathbf{x}}_k^s} = (\mathbf{Q}_{\hat{\mathbf{x}}_{k,k-1}^s}^{-1} + \mathbf{Q}_{\mathbf{x}_k^s}^{-1})^{-1}, \tag{11}$$

165 with the parameter being also updated with the epoch-wise estimate and its variance-covariance

$$\hat{\mathbf{x}}_k^s = \hat{\mathbf{x}}_{k-1}^s + \mathbf{Q}_{\hat{\mathbf{x}}_k^s} \mathbf{Q}_{\mathbf{x}_k^s}^{-1} (\mathbf{x}_k^s - \hat{\mathbf{x}}_{k-1}^s), \tag{12}$$

166 where elements of $\hat{\mathbf{x}}_k^s$ and $\mathbf{Q}_{\hat{\mathbf{x}}_k^s}$ are used to derive the WL ambiguity, i.e.

$$\hat{\tilde{N}}_{wl,r}^s = \hat{\tilde{N}}_{1,r}^s - \hat{\tilde{N}}_{2,r}^s, \tag{13}$$

167 with its formal error being derived

$$\sigma_{\hat{\tilde{N}}_{wl,r}^s} = \sqrt{\sigma_{\hat{\tilde{N}}_{1,r}^s}^2 + \sigma_{\hat{\tilde{N}}_{2,r}^s}^2 - 2 \cdot \sigma_{\hat{\tilde{N}}_{1,r}^s, \hat{\tilde{N}}_{2,r}^s}}, \tag{14}$$

168 where $\sigma_{\hat{\tilde{N}}_{1,r}^s}^2, \sigma_{\hat{\tilde{N}}_{2,r}^s}^2, \sigma_{\hat{\tilde{N}}_{1,r}^s, \hat{\tilde{N}}_{2,r}^s}$ are taken from $\mathbf{Q}_{\hat{\mathbf{x}}_k^s}$.

169 ### 3. WL ambiguities derived from the GB model

170   To derive the ambiguities from the GB model, we assume that the station coordinates
171 (X_r, Y_r, Z_r), satellite orbit $(X^s(k), Y^s(k), Z^s(k))$ and clock errors $\delta t_{if}^s(k)$ are precisely known. As we
172 know that the satellite clock errors are calculated from ionosphere-free combination observations [2]:

$$\delta t_{if}^s(k) = \delta t^s(k) + \frac{\mu_2}{\mu_2 - \mu_1} d_{p_1}^s - \frac{\mu_1}{\mu_2 - \mu_1} d_{p_2}^s, \tag{15}$$

173 and the computed range between satellite and the known station coordinates is

174
$$\rho_r^s(k) = \sqrt{\{X^s(k) - X_r\}^2 + \{Y^s(k) - Y_r\}^2 + \{Z^s(k) - Z_r\}^2}$$

175   Add Equation (15) to Equation (1), insert $\rho_r^s(k)$ the left side, and define the observed minus
176 computed values as:

$$\begin{aligned}
\delta p_{i,r}^s(k) &:= p_{i,r}^s(k) - \rho_r^s(k) + \delta t_{if}^s(k) \\
\delta \varphi_{i,r}^s(k) &:= \varphi_{i,r}^s(k) - \rho_r^s(k) + \delta t_{if}^s(k)
\end{aligned}, \tag{16}$$

177 resulting in the following:

$$\begin{aligned}
E\{\delta p_{i,r}^s(k)\} &= m_r^s T_r + t_r(k) + \mu_i \tilde{I}_r^s(k) \\
E\{\delta \varphi_{i,r}^s(k)\} &= m_r^s T_r + t_r(k) - \mu_i \tilde{I}_r^s(k) + \lambda_i \tilde{N}_{i,r}^s
\end{aligned}, \tag{17}$$

178 Where the ionosphere and ambiguity terms are defined as the same as in Equations (3) and (4),
179 respectively, and the receiver clock term is defined as:

$$t_r(k) := \delta t_r(k) + \frac{\mu_2}{\mu_2 - \mu_1} d_{p_1, r} - \frac{\mu_1}{\mu_2 - \mu_1} d_{p_2, r}$$

180

181   The observation equations of all observed satellites in the matrix-vector form can be expressed
182 as:

$$\mathbf{y}_k = \mathbf{A}_k\,\widetilde{\mathbf{x}}_k + \boldsymbol{\varepsilon}\ , \tag{18}$$

183 where $\widetilde{\mathbf{x}}_k := \begin{bmatrix} T_r & t_r(k) & \mathbf{I}_r(k) & \mathbf{N}_{1,r} & \mathbf{N}_{2,r} \end{bmatrix}^T$ with $\mathbf{I}_r(k) := \begin{bmatrix} \widetilde{I}_r^1(k) & \widetilde{I}_r^2(k) & \cdots & \widetilde{I}_r^m(k) \end{bmatrix}^T$ and

184 $\mathbf{N}_{i,r}(k) := \begin{bmatrix} \widetilde{N}_{i,r}^1 & \widetilde{N}_{i,r}^2 & \cdots & \widetilde{N}_{i,r}^m \end{bmatrix}^T$, $\mathbf{y}_k := \begin{bmatrix} \mathbf{P}_{1,r} & \mathbf{P}_{2,r} & \Phi_{1,r} & \Phi_{2,r} \end{bmatrix}^T$ with $\mathbf{P}_{i,r} := \begin{bmatrix} \delta p_{i,r}^1 & \delta p_{i,r}^2 & \cdots & \delta p_{i,r}^m \end{bmatrix}^T$ and

185 $\Phi_{i,r} := \begin{bmatrix} \delta\varphi_{i,r}^1 & \delta\varphi_{i,r}^2 & \cdots & \delta\varphi_{i,r}^m \end{bmatrix}^T$; $\mathbf{A}_k$ is the design matrix with its elements being formed with the

186 coefficients in Equation (17) for all visible satellites.

187 The stochastic model is expressed as :

$$\boldsymbol{\varepsilon} \sim N(0,\mathbf{Q}_{\mathbf{y}_k})\ , \tag{19}$$

188 where $\mathbf{Q}_{\mathbf{y}_k} = diag\{\sigma(e)_p^2 \quad \sigma(e)_p^2 \quad \cdots \quad \sigma(e)_p^2 \quad \sigma(e)_\phi^2 \quad \sigma(e)_\phi^2 \quad \cdots \quad \sigma(e)_\phi^2\}$.

189 It is noticed that the observation equation (18) has redundancy when the number of satellites is
190 larger than three, which is easy to achieve even when only GPS satellites are employed. The state
191 transition equation is given by

$$\widetilde{\mathbf{x}}_k = \mathbf{B}\widetilde{\mathbf{x}}_{k-1} + \mathbf{w}\ , \tag{20}$$

192 where $\mathbf{B} := \begin{bmatrix} 1 & 0 & \mathbf{0}_m^T & \mathbf{e}_m^T & \mathbf{e}_m^T \end{bmatrix}^T$ with $\mathbf{e_m} := \begin{bmatrix} 1 & 1 & \cdots & 1 \end{bmatrix}^T$ and $\mathbf{w} \sim N(0,\mathbf{Q_w})$, which links the
193 troposphere and ambiguity parameters with that of previous epochs.

194 Assume that the filtering solution at the epoch k-1 is denoted as $\hat{\widetilde{\mathbf{x}}}_{k-1}$ with its covariance matrix
195 $\mathbf{Q}_{\hat{\widetilde{\mathbf{x}}}_{k-1}}$, the solution at the epoch k is computed as:

$$\hat{\widetilde{\mathbf{x}}}_k = \hat{\widetilde{\mathbf{x}}}_{k,k-1} + \mathbf{K}_k(\mathbf{y}_k - \mathbf{A}_k\hat{\widetilde{\mathbf{x}}}_{k,k-1})\ , \tag{21}$$

196 with its covariance matrix being computed as

$$\mathbf{Q}_{\hat{\widetilde{\mathbf{x}}}_k} = (\mathbf{I} - \mathbf{K}_k\mathbf{A}_k)\mathbf{Q}_{\hat{\widetilde{\mathbf{x}}}_{k,k-1}}\ , \tag{22}$$

197 where $\hat{\widetilde{\mathbf{x}}}_{k,k-1} = \mathbf{B}\hat{\widetilde{\mathbf{x}}}_{k-1}$, and its covariance matrix as $\mathbf{Q}_{\hat{\widetilde{\mathbf{x}}}_{k,k-1}} = \mathbf{B}\mathbf{Q}_{\hat{\widetilde{\mathbf{x}}}_{k-1}}\mathbf{B}^T + \mathbf{Q_w}$, and the gain matrix is
198 computed as $\mathbf{K}_k = \mathbf{Q}_{\hat{\widetilde{\mathbf{x}}}_{k,k-1}}\mathbf{A}_k^T(\mathbf{A}_k\mathbf{Q}_{\hat{\widetilde{\mathbf{x}}}_{k,k-1}}\mathbf{A}_k^T + \mathbf{Q}_{\mathbf{y}_k})^{-1}$.

199 The L1 and L2 ambiguities with their covariance matrix can be used to derive the GB WL
200 ambiguity and its formal error as Equations (13) and (14) for their GF counterparts.

4. Impact of orbit and clock residual errors on ambiguity estimation

202 From Equations (5) and (17), there is no difference between the GF and GB ambiguities in terms
203 of parameterization. However, their estimates are different since they go through different estimation
204 procedures. For the GF ambiguities, the geometry related terms, including orbit and clock, are
205 eliminated without effects. However it results in no redundancy for the epoch-wise estimates. The
206 solution's accuracy is dominated by the noise of code measurements. In this case, the solution with
207 multiple epochs is computed. For the GB ambiguities, the geometry strength is higher (as there are
208 redundancy in each epoch), the ambiguities converge quicker than the GF ones. However, the
209 observed minus computed values are computed from the orbit and clock, which are not always
210 precise enough. The orbit and clock residual error at the LOS remains in the observation as follows:

$$E\{\delta p_{i,r}^s(k)\} = m_r^s T_r + t_r(k) + \mu_i\widetilde{I}_r^s(k) + oc_r^s$$
$$E\{\delta\varphi_{i,r}^s(k)\} = m_r^s T_r + t_r(k) - \mu_i\widetilde{I}_r^s(k) + \lambda_i\widetilde{N}_{i,r}^s + oc_r^s \tag{23}$$

211 where oc_r^s indicates the slowly time-variant or time-invariant residual part of orbit and clock error
212 combination in the LOS direction. As they are not random noise, they could be distributed to every
213 parameters (as well as measurement residuals), but most likely to the ionosphere and ambiguity

214 terms of the satellite as these parameters are satellite dependent. There are two cases worthy of
215 investigation.

4.1. Orbit and clock residual error being *time-constant bias*

217 It is possible that the orbit and clock contain a constant bias. For example, the code measurement
218 type used in mobile side is not consistent with the code measurements used in the reference side
219 when computing the clock products. It is assumed that the oc_r^s is a constant during the whole
220 measurement period and there are no effects between satellites. As phase measurements are assigned
221 much higher weight than code ones (100 times smaller in terms of standard deviation), we assume
222 no significant orbit and clock errors are attributed to phase measurement residuals. Furthermore, the
223 ambiguities are common terms between epochs, they likely absorb the constant bias as:

$$
\begin{aligned}
\widetilde{\widetilde{N}}_{1,r}^s &:\approx \widetilde{N}_{1,r}^s + \frac{1}{\lambda_1} \frac{\mu_1 + 3\mu_2}{2\mu_2} oc_r^s \ , \\
\widetilde{\widetilde{N}}_{2,r}^s &:\approx \widetilde{N}_{2,r}^s + \frac{1}{\lambda_2} \frac{3\mu_1 + \mu_2}{2\mu_1} oc_r^s
\end{aligned}
\tag{24}
$$

224 The remaining error may be distributed to the ionosphere term and the code residuals. From the
225 analytical expression of Equation (24), the effect on the WL ambiguity term is less than one tenth of
226 oc_r^s in terms of cycle. In other words, the effect of constant bias in orbit and clock looks largely
227 reduced. Bearing in mind that the reality can be more complex when our assumptions do not hold
228 for all cases. In particular, the geometry changing may have influence as well. However, the effects
229 of a constant bias analyzed here might be a minimum (i.e. a bottom line).

4.2. Orbit and clock residual error being time-variant error

231 The residual orbit and clock error is rarely a constant bias in an entire tracking period, except for
232 a mixture use of code measurements. It is very likely a time variant error that caused by the changes
233 of LOS and the orbit error itself (as will be shown later). In this case, it is not a trivial to make a strict
234 analytical expression, as the estimation procedure is rather complex both in current epoch and
235 correlation between epochs. Assume that the error is directly mapped to the ambiguity terms as
236 follows:

$$
\begin{aligned}
\widetilde{\widetilde{N}}_{1,r}^s &:\approx \widetilde{N}_{1,r}^s + \frac{1}{\lambda_1} oc_r^s \ , \\
\widetilde{\widetilde{N}}_{2,r}^s &:\approx \widetilde{N}_{2,r}^s + \frac{1}{\lambda_2} oc_r^s
\end{aligned}
\tag{25}
$$

237 where the effect on WL ambiguity term will be about $1.165 \cdot oc_r^s$ cycle. In other words, one meter bias
238 could bring 1.165 cycle error into the WL ambiguity. Even when the error is about 15 cm (often the
239 case for real-time orbit and clock), the effects will be significantly up to 0.18 cycle, which is not
240 acceptable for phase bias calibration for PPP IAR. In reality, the effects might be around (larger or
241 smaller than) this level due to different geometry strength. This contribution will make a real-data
242 numerical analysis in order to further understand the effects.

5. Experiment and results analysis

244 In order to analyze the performance of GF and GB WL ambiguities and evaluate the orbit and
245 clock effects on the WL ambiguities, we implemented the GF and GB models using raw observations
246 to compute L1, L2 and WL ambiguities as well as their variance-covariance as described in "WL
247 ambiguities derived from the GF model" and "WL ambiguities derived from the GB model". GNSS
248 measurements with 1 second interval from selected IGS sites are downloaded from the IGS data base.
249 These sites are deliberately selected and spread over main continents and the middle of the Pacific in
250 terms of groups, see Figure 1. Some of groups have sites located at very nearby in order to have
251 almost the same LOS. Two types of orbit and clock products are used in the experiment. One type is

252 the determined orbit and clock products provided by ESA to the IGS, while the other is the real-time
253 orbit and clock estimated as described in [15]. The interval of satellite orbit is 15 min, and the sample
254 rate of satellite clock is 30 s for both types of products. The determined products are obtained by the
255 post-processing mode, and their accuracy is better than that of real-time ones [15]. The standard GB
256 PPP solutions, in parallel with the GF process, are computed using raw L1 and L2 observations. The
257 parameters to be estimated are tropospheric zenith delay, ionosphere, receiver clock bias, and L1, L2
258 and then WL ambiguity terms for the GB process, while the GF process just produces the L1, L2 and
259 then WL ambiguity terms. The positions of sites are fixed to the "ground truth", which are computed
260 from many days' data with the static mode. This contribution makes use of the precise coordinates
261 in order to determine precisely the GB-GF ambiguities by avoiding of the effects of unknown
262 coordinates. The orbit and clock are integrated and interpolated for each epoch (1 s of data interval).
263 Strictly speaking, the interpolation for real-time orbit and clock is not realistic in the real-time
264 application as the future correction stream cannot be known in advance for interpolation of current
265 epoch. However, we employ exactly the same process in order to carry out a fair comparison for both
266 types of products by ignoring correction age effects. The elevation-dependent data weighting is used
267 for both processes. The entire process is implemented through a strictly forward computation.

268
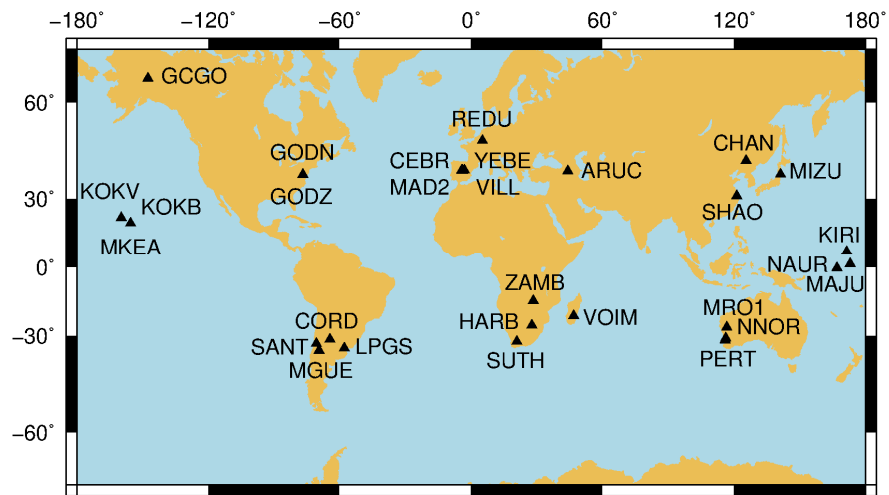
269   **Figure 1.** Distribution of sites that are used for this study

270 *5.1. Analysis of GB and GF ambiguities*

271   This section will analyze the GB and GF ambiguities and inspect the similarity and discrepancies
272 of GB and GF WL ambiguities.

273   Figure 2 shows L1, L2 and WL ambiguities and their corresponding formal standard deviations
274 for PRN 09. These ambiguities are respectively produced with the GF and GB models for site CEBR.
275 Arbitrary offsets are removed from these ambiguities. It is obvious that both the variation of L1 and
276 L2 GF ambiguities and their formal errors are larger than the GB counterparts, and especially they
277 converge much slower than that of GB. However, the formal errors of WL ambiguities are very
278 consistent and almost the same, meanwhile their estimates reveal a consistent trend despite of some
279 small fluctuations. This confirms the analytical statement in [19] that the GF WL ambiguity precision
280 does not differ too much from its GB counterpart. The reason is that the GF L1 and L2 ambiguities
281 are highly correlated and even more correlated than that of GB ones. The WL ambiguities are
282 therefore much precise after the differential operator, referring to (13)-(14), compared with the L1 and
283 L2 ones. It is noticed that the GF WL ambiguities are slightly oscillated, compared with the GB ones
284 at the first hour, but they are even stable than the GB ones afterwards. The reason is that the GB WL
285 ambiguities may suffer some errors in orbit and clock. This will be further analyzed in other sections.

286
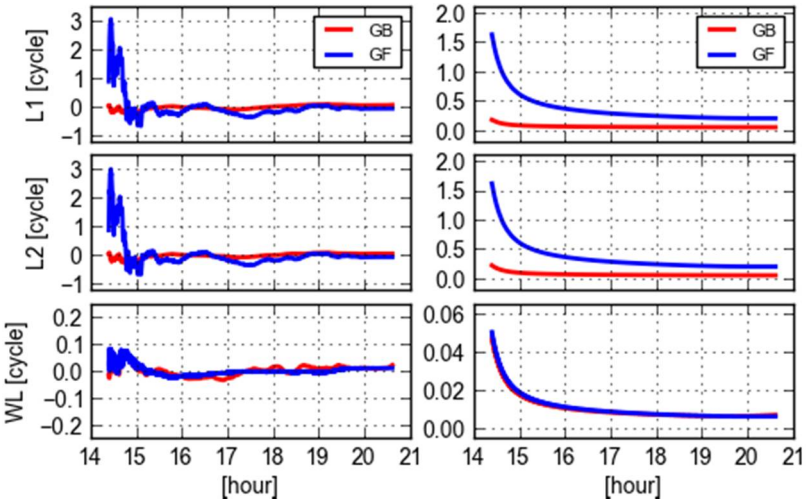
287　　**Figure 2.** GF (blue) and GB (red) L1, L2 and WL ambiguities (left) and their corresponding formal
288　　errors (right) of PRN 09 computed from a single receiver (CEBR) observations and ESA final orbit and
289　　clock products

290　　　　As can be seen from Figure 3 that the results of PRN 09 computed by another single receiver
291　　REDU have similar behavior to that of CEBR, which indicates that the WL ambiguities and their
292　　formal errors have commonality for this same satellite obtained by different receivers which are
293　　located not very far away.

294
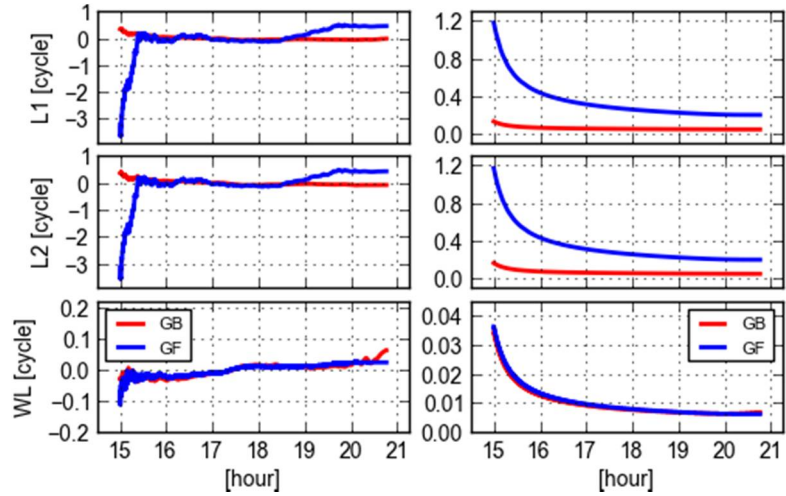
295　　**Figure 3.** GF (blue) and GB (red) L1, L2 and WL ambiguities (left) and their corresponding formal
296　　errors (right) of PRN 09 computed using a single receiver (REDU) observations and ESA final orbit
297　　clock products

298　　　　Figure 4 displays the differences of GB and GF WL ambiguities and their computed standard
299　　deviations derived from GB and GF ones using the error propagation law for PRN 09 at the site CEBR
300　　and REDU, respectively. The values of GB-GF are stable in between ± 0.1 cycles. The variation at the
301　　first hour is largely dominated by the GF ambiguities, while it changes due to the variation of GB
302　　ambiguities afterwards. The variations of GB-GF values are mostly within three times of the formal
303　　errors, which indicates that the formal errors statistically reflect the level of quality.

304
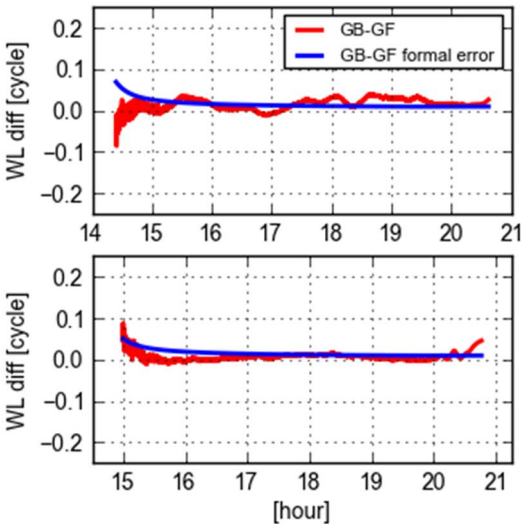
305   **Figure 4.** Differences of GB and GF WL ambiguities (red) and their formal errors (blue) of PRN 09
306   from the receivers CEBR (top) and REDU (bottom).

307   Figure 5 displays the values of GB-GF WL ambiguities computed with ESA final orbit and clock
308   products at site KOKV for all visible GPS satellites. It is seen that these values are stable and close to
309   zero. Again, the typical behavior of these time series is that they are noisy at the beginning of a
310   tracking period, but become smooth and stable afterwards. According to the statistics, the biases are
311   smaller than 0.05 cycle and the standard deviations of these values are smaller than 0.025 cycle. It is
312   practically and commonly believed that the repeatability is good enough if   differences of
313   ambiguities are smaller than 0.1 cycle [7]. Therefore, we could state that the GB and GF WL
314   ambiguities are equivalent in this case, though they are not the same.

315
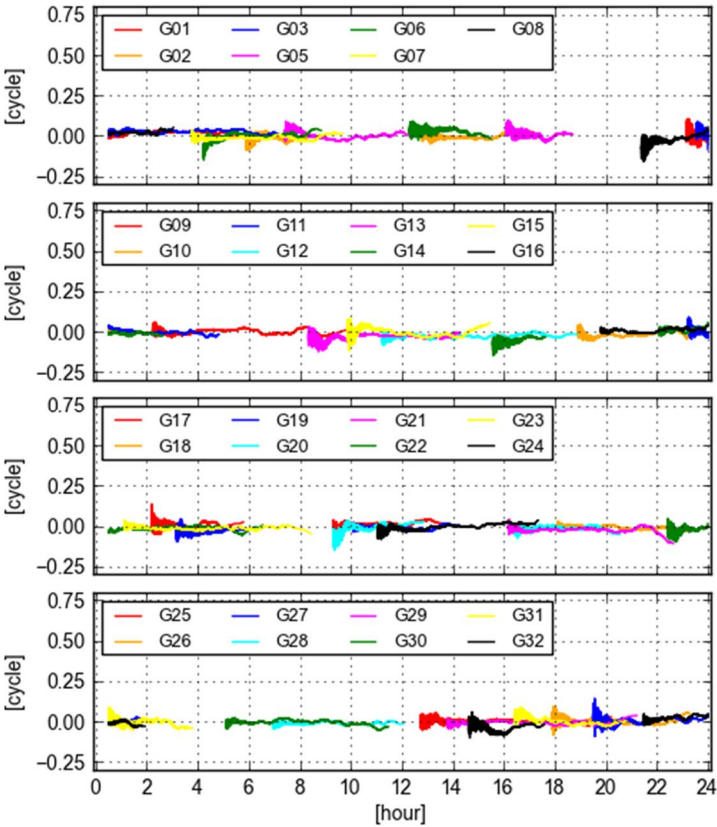
316   **Figure 5.** Differences of GB and GF WL ambiguities computed with ESA final orbit and clock products
317   at site KOKV

5.2. Orbit and clock residual error effects

319   The results demonstrated in previous section are computed with the ESA final orbit and clock
320   products. To compare with them, this section will show results that are computed with the real-time
321   orbit and clock products.
322   Figure 6 displays various differences of PRN 09 WL ambiguities and orbit clock products
323   computed at the site CEBR and REDU, respectively. In top panels, the GF WL differences are zeros
324   as the orbit and clock are eliminated and have no impact on the GF ambiguity estimates. The GB WL
325   differences are computed with final and real-time orbit and clock. In this case, everything is the same
326   except that the orbit and clock used are different. Therefore, the GB WL differences indicate that the
327   effects of the different orbit and clock products. To further confirm this, the differences of two types
328   of orbit and clock are also computed for the locations of the receivers, in which the orbits are mapped
329   into the LOS direction. The values are converted to cycles by divided with the wavelength of WL
330   ambiguities (which is 86.2 cm). It is clear that the variations of two sets of orbit and clock differences
331   are largely coincide with the differences of GB WL ambiguities.   In bottom panels, the GB minus GF
332   WL ambiguities used two types of orbit and clock products are shown together with the orbit and
333   clock differences themselves. The values of GB-GF computed from the final orbit and clock (OC1:
334   GB-GF in the figure) are more stable than that of computed from the real-time orbit and clock (OC2:
335   GB-GF in the figure). The latter one has a clear slope in the time series, which is consistent with the
336   slope of orbit and clock differences. In this case, it is difficult to say the GF WL ambiguities are
337   equivalent with the GB ones. However, it is promising for the real-time users that the GB-GF WL
338   ambiguities can be used to an indicator of the orbit and clock quality from a user's perspective.

339
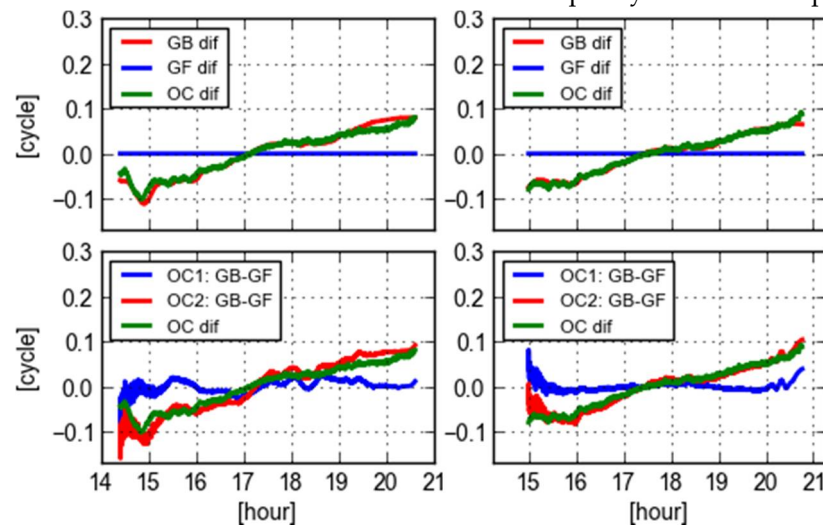
340   **Figure 6.** Various differences of PRN 09 WL ambiguities and orbit clock products computed at the
341   receiver CEBR (left) and REDU (right): 1) differences of GB ambiguities computed with final and real-
342   time orbit clock products are indicated in red in top panels; 2) differences of GF ambiguities computed
343   with final and real-time orbit clock products are indicated in blue in top panels; 3) differences of GB
344   and GF ambiguities computed with final orbit clock products (OC1) are indicated in blue in bottom
345   panels; 4) differences of GB and GF ambiguities computed with real-time orbit clock products (OC2)
346   are indicated in red in bottom panels; 5) differences of orbit clock impacts in LOS directions between
347   final and real-time orbit clock products in green

348   Figure 7 displays the values of GB - GF WL ambiguities computed with real-time orbit and clock
349   products at site KOKV for all visible GPS satellites. During the period of 2-12 O'clock, the variations
350   of these time series are larger than the rest of day. In particular, the largest variation is from PRN 09,
351   which is even larger than 1.0 cycle during 9-10 O'clock. The bias and the standard deviation are -0.569

352   and 0.305 cycle according to the statistics. In this case, the GB and GF WL ambiguities are not
353   equivalent.

354
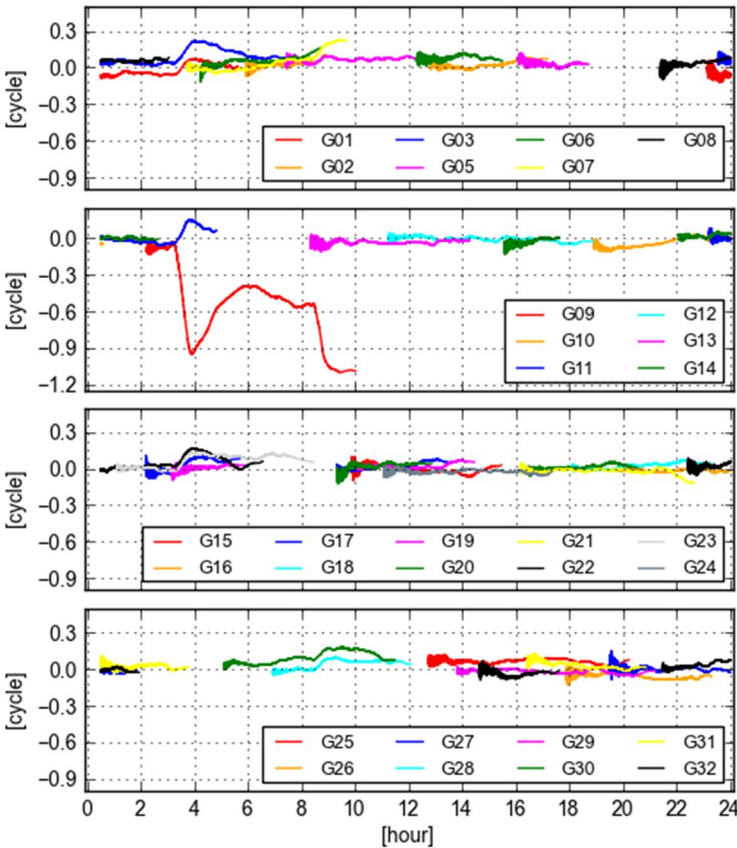
Figure 7. Differences of GB - GF WL ambiguities computed with real-time orbit and clock products at Site KOKV

357   To further investigate the cause of the variation in GB-GF WL ambiguities, we plot the variations
358   of differences between the final and real-time orbit clock (orbit is projected into the LOS) at Site KOKV
359   for all visible GPS satellites in figure 8. It is clearly seen that the pattern of the orbit and clock
360   differences is very similar with that of GB-GF ambiguities, in particular, for the satellite PRN 09. The
361   reason for such an extreme orbit and clock behavior in real-time is likely that the orientation of the
362   satellite (mainly IIF satellites) is estimated or predicted wrongly [22]. This issue has not been solved
363   in real-time case. Therefore, it is valuable that the variation of GB-GF values of a receiver can be taken
364   as a quality index of orbit clock products from users' perspective.

365
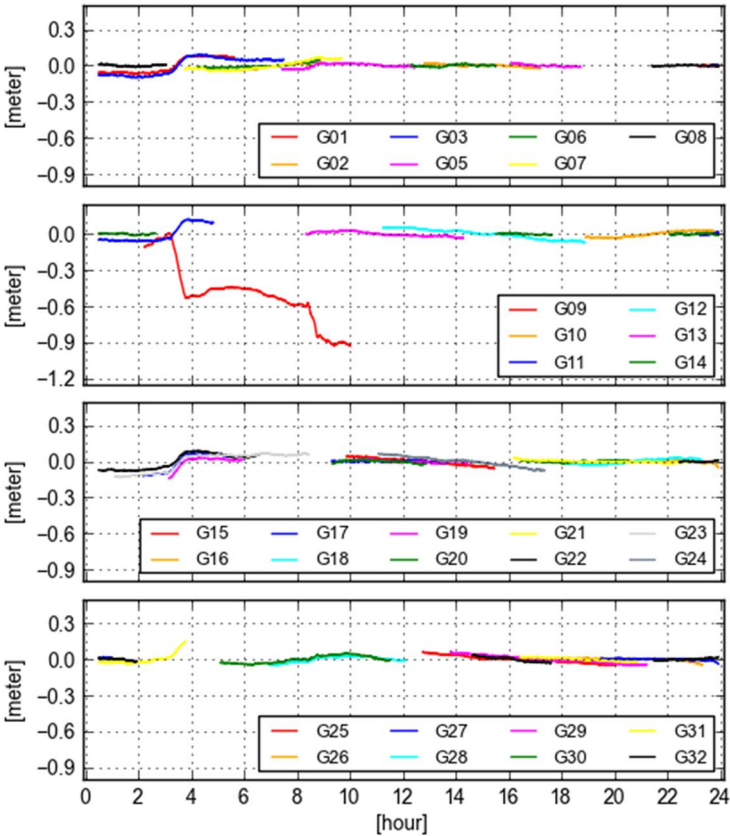
Figure 8. Variations of final orbit/clock and real-time orbit/clock differences projected into the LOS at Site KOKV for all visible GPS satellites

Figure 9 displays GB-GF WL ambiguities of PRN 09 computed with real-time orbit clock products for all selected sites. It is obvious that these time series are not stable. The figure discloses longer period of oscillations than one single site shown in figure 7. We could also see that the variation patterns are almost the same for some pairs of sites, e.g. KOKB and KOKV, KIRI and NAUR, MIZU and SANT, MRO1 and PERT. These pairs of sites have different observations, but demonstrate the same GB-GF WL patterns, as they suffer almost the same orbit clock error. It is clear in this case that the GB and GF WL ambiguities are not equivalent.

375
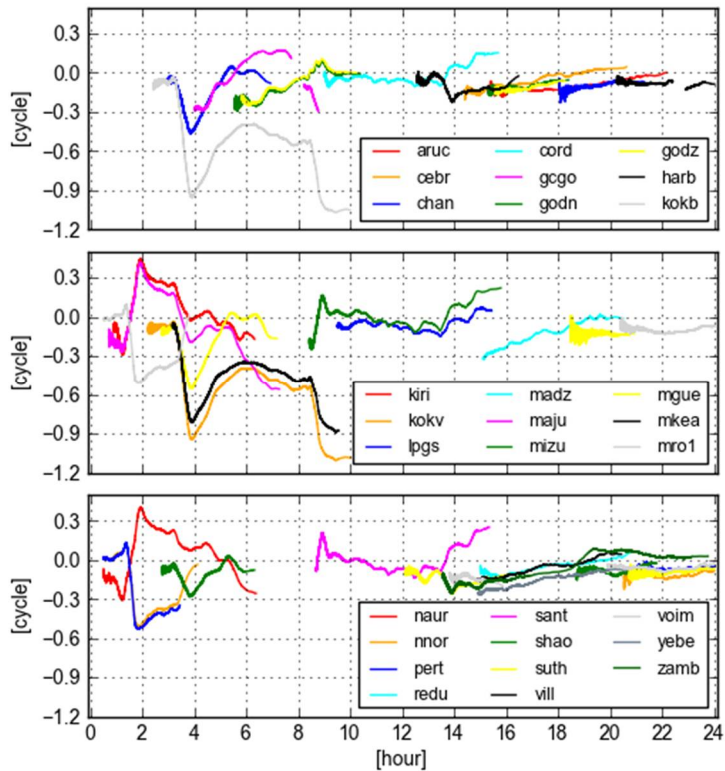
Figure 9. GB - GF WL ambiguities computed with real-time orbit clock products for GPS PRN 09 at
all selected sites

6. Simulation study of orbit/clock error effects

In order to further investigate the effects of orbit and clock errors on the WL ambiguities, we simulate two types of errors directly in the LOS for one satellite of an entire tracking period at Site KOKV: 1) a constant bias (e.g. 1.0 m); 2) time-variant errors with 0.15 m amplitude and 2 hours period of sine or cosine changes. The errors are added to only PRN 30 of the ESA final orbit and clock. The GB-GF WL ambiguities are then recomputed and compared with the previous ones. The purpose for such a simulation is to see how effects of precisely "known errors" on the GB-GF ambiguities.

Figure 10 displays differences of recomputed GB-GF WL ambiguities with respect to their counterparts without the simulated errors. The differences are purely caused by the simulated errors. The top panel displays the GB-GF WL effects of a 1.0 m constant bias is added into the PRN 30 during 5:00 h – 11:30 h. The effect is about a constant bias of 0.084 cycle. There is no visible effects on other satellites. This indicates that the GB-GF WL ambiguity is not very sensible to a constant bias, which confirms the analysis in "orbit and clock residual error being constant bias".

391
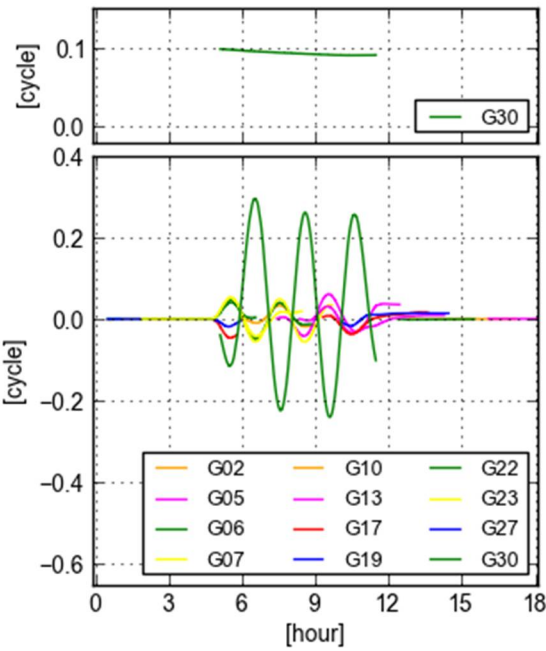
Figure 10. Recomputed GB-GF WL ambiguities minus the previous ones in figure 5 with the simulated constant bias (top) and the time-variant errors (bottom) added into orbit clock of PRN 30 at Site KOKV

The bottom panel demonstrates the GB-GF WL effects after the time-variant errors are added into the PRN 30 during 5:00 h – 11:30 h. Firstly, the effects of PRN 30 show also the sine or cosine behavior. Secondly, there are also similar patterns with smaller magnitude in many other satellites tracked in the same period. These effects are brought by the added errors with only 0.15 m in (absolute) size, which is much smaller than 1.0 m. This indicates that the GB-GF WL ambiguity is very sensible to time-variant errors as analyzed in "orbit and clock residual error being time-variant error", which provides an opportunity for real-time user to evaluate the quality of real-time orbit and clock.

7. Conclusions

This contribution derives L1, L2 and WL ambiguities from the GF and GB PPP model. Two types of orbit and clock products, represented different level of quality, are used to compute the WL ambiguities. The differences of GB and GF WL ambiguities are particularly analyzed. The main results and conclusions are summarized in the following.

The GF ambiguities are obtained on individual satellite basis, and there is no redundancy for the epoch-wise estimation. To improve GF estimates, multiple epochs of data are needed. The GB ambiguity estimation makes use of all received satellites, therefore the geometry and the redundancy, besides using multiple epochs of data, play roles on the estimation. From our implementation and experiment, there are significant differences between GB L1/L2 ambiguities and the GF ones in terms of both estimates and their precisions, however, the GB WL ambiguities do not differ much from the GF ones in terms of precision at least.

Orbit and clock have no impact on GF WL ambiguities as they are eliminated in the process, while they have effects on GB ones. Whether the GB and GF ambiguities are equivalent depends much on the quality of the used orbit and clock. In general, if GB-GF WL values are stably in between ± 0.1 cycles or within three times of their formal errors, we could state that the GB and GF WL ambiguities are equivalent. This is basically not an issue for the final orbit and clock product used in our experiment, as this type of product is obtained from post-processing.

The GB and GF WL ambiguities are not always equivalent if they are computed from the real-time orbit and clock, as the type of product is sometimes not perfect. It is found in this contribution

423   that the variation of GB-GF WL ambiguities are coincide with the orbit and clock differences between
424   the final and real-time products. Therefore, it is promising for the real-time users that the GB-GF WL
425   ambiguities can be directly used to indicate the orbit and clock quality from a user's perspective.
426   Two types of orbit and clock errors are simulated and the effects on GB-GF WL ambiguities are
427   analyzed. The constant bias in orbit and clock seems not have significant effects on GB-GF WL values
428   if we look into the pattern of their time-series, though there is still a smaller size of bias presenting.
429   This indicates that the GB-GF WL ambiguity is not very sensible to a constant bias in orbit and clock.
430   However, the GB-GF WL ambiguity varies remarkably if the time- variant errors exist in the orbit
431   and clock. Even the errors are not large, it is sensitively mapped into GB-GF WL ambiguities. As this
432   type of errors is more often showing up than the constant bias in the real-time orbit and clock, the
433   GB-GF WL ambiguity provides an opportunity for real-time users to evaluate the quality of real-time
434   orbit and clock.

435   **Author Contributions:** G.C. provided the initial concept and methodology; Q.Z. helped to derive the equations
436   in theory with G.C.; G.C acquired the funding for the project and carried out the data processing. Q.Z. provided
437   the software platform and results analysis. S.L. implemented the software part necessarily for this project and
438   carried out the experimental validation; S.L. visualized the results and wrote the draft of the paper. G.C. and
439   Q.Z. finalized the paper. All authors reviewed the paper.

440   **Funding:** This research was funded by the National Natural Science Foundation of China (Grant NO. 41674015,
441   41274035, 41774036, 41574030).

442   **Acknowledgments:** The IGS is greatly acknowledged for providing GNSS raw data and precise orbit and clock.

443   **Conflicts of Interest:** The authors declare no conflict of interest.

References

445   1.   Zumberge JF; Heflin MB; Jefferson DC; Watkins MM; Webb FH. Precise point positioning for the efficient
446   and robust analysis of GPS data from large networks. *J Geophys Res* **1997**, *102(B3)*, pp.5005-5017,
447   DOI:10.1029/96JB03860
448   2.   Kouba J; Heroux P. Precise point positioning using IGS orbit products. *GPS Solut* **2001**,*5(2)*,pp.12–28
449   3.   Geng J; Teferle FN; Shi C; Meng X; Dodson FN; Liu J. Ambiguity resolution in precise point positioning
450   with hourly data. *GPS Solut* **2009**, *13(4)*, pp.263–270
451   4.   Muellerschoen RJ; Iijima B; Meyer R; Bar-Server Y; Accad E. Real-time point-positioning performance
452   evaluation of single-frequency receivers using NASA's global differential GPS system. Proceedings of ION
453   GNSS 17th international technical meeting of the Satellite Division, 21-24 September 2004, Long Beach, CA,
454   USA, pp.1874–1880
455   5.   Leandro R et al. RTX positioning: the next generation of cm-accurate real-time GNSS positioning.
456   Proceedings of the 24th International Technical Meeting of the Satellite Division of the ION, 20-23
457   September 2011,Portland Oregon, pp.1460-1475
458   6.   Li X; Ge M; Dai X; Ren X. Accuracy and reliability of multi-GNSS real-time precise positioning: GPS,
459   GLONASS, BeiDou, and Galileo. *J Geod* **2015**, *89(5)*, pp.607-635. DOI: 10.1007/s00190-015-0802-8
460   7.   Ge M; Gendt G; Rothacher M; Shi C; Liu J. Resolution of GPS carrier phase ambiguities in precise point
461   positioning (PPP) with daily observations. *J Geod* **2008**, *82(7)*, pp.389–399
462   8.   Laurichesse D; Mercier F; Berthias JP. Zero-difference integer ambiguity fixing on single frequency
463   receivers. Proceedings of ION ITM-2009, Anaheim, 26–28 January 2009, pp.2460–2469
464   9.   Collins P; Bisnath S; Lahaye F; Heroux P. Undifferenced GPS ambiguity resolution using the decoupled
465   clock model and ambiguity datum fixing. *Navigation* **2010**,*57(2)*, pp.123–135
466   10. Geng J; Shi C; Ge M; Dodson AH; Lou Y; Zhao Q; Liu J. Improving the estimation of fractional-cycle biases
467   for ambiguity resolution in precise point positioning. *J Geod* **2012**,*86(8)*, pp.579–589
468   11. Li X; Li X; Yuan Y; Zhang K; Zhang X; Wickert J. Multi-GNSS phase delay estimation and PPP ambiguity
469   resolution: GPS, BDS, GLONASS, Galileo. *J Geod* **2017**, DOI: 10.1007/s00190-017-1081-3
470   12. Wübbena G; Schmitz M; Bagge A. PPP-RTK: precise point positioning using state-space representation in
471   RTK networks. Proceedings of ION GNSS 18th international technical meeting of the Satellite Division, The
472   Institute of Navigation, Inc., September 2005, Fairfax, USA, pp.2584–2594

13. Teunissen PJG; Odijk D; Zhang B. PPP-RTK: results of CORS network-based PPP with integer ambiguity resolution. *Journal of Aeronautics Astronautics & Aviation* **2010**, *42(4)*, pp.223–230

14. Li X; Ge M; Zhang H; Wickert J. A method for improving uncalibrated phase delay estimation and ambiguity-fixing in real-time precise point positioning. *J Geod* **2013,** *87*, pp.405-416. DOI: 10.1007/s00190-013-0611-x

15. Chen G; Zhao Q. Near-field surface displacement and permanent deformation induced by the Alaska Mw 7.5 earthquake determined by high-rate real-time ambiguity-fixed PPP solutions. *Chin. Sci. Bull* **2014**, *59(34)*, pp.4781-4789. DOI: 10.1007/s11434-014-0609-7

16. Hatch R. The Synergism of GPS code and carrier measurements. Proceedings of the third international symposium on satellite Doppler positioning at physical sciences laboratory of New Mexico State University, 8-12 February 1982, *Vol. 2*, pp.1213-1231

17. Melbourne W. The case for ranging in GPS-based geodetic systems. Proceedings of First international symposium on precise positioning with the global positioning system,1985, Rockville, pp.373–386

18. Wübbena G. Software developments for geodetic positioning with GPS using TI-4100 code and carrier measurements. Proceedings of First international symposium on precise positioning with the global positioning system, 1985, Rockville, pp 403–412

19. Teunissen PJG; Khodabandeh A. Review and principals of PPP-RTK methods. *J Geod* **2015** *89(3)*, pp.217-240. DOI: 10.1007/s00190-014-0771-3

20. Montenbruck O et al. The multi-GNSS experiment (MGEX) of the international GNSS service (IGS) – Achievements, prospects and challenges. *Adv Space Res* **2017**, *59(7)*, pp.1671-1697

21. Kazmierski K; Sosnics K; Hadas T. Quality assessment of multi-GNSS orbits and clocks for real-time precise point positioning. *GPS Solut* **2018**, *22(1)*, pp.11. DOI: 10.1007/s10291-017-0678-6

22. Dilssner F; Springer T; Schoenemann; Zandbergen R; Enderle W. How GNSS spacecraft orientation error affect solar radiation pressure modelling. Presentation in EGU 2015, Vienna, Austria.

23. Kouba J. A simplified yaw-attitude model for eclipsing GPS satellites. *GPS Solut* **2009**, *13(1)*, pp.1-12

24. Lou Y; Zhang W; Wang C; Liu J. The impact of orbital errors on the estimation of satellite clock errors and PPP. *Adv Space Res* **2014**, *54(8)*, pp.1571-1580

25. Pan S; Chen W; Jin X; Shi X; He F. Real-time PPP based on the coupling estimation of clock bias and orbit error with broadcast ephemeris. *Sensors* **2015**, *15(7)*, pp.17808-17826; DOI:10.3390/s150717808

26. Teunissen P. Basic Observation Equations. In *Springer Handbook of Global Navigation Satellite Systems*, 2nd ed.; Teunissen P., Montenbruck O., Eds.; Springer Nature: Cham, Switzerland, 2017; pp.561-573, 978-3-319-42926-7.

27. Khodabandeh A; Teunissen PJG. An analytical study of PPP-RTK corrections: precision, correlation and user-impact. *J Geod* **2015**, *89(11)* pp.1109-1132. DOI: 10.1007/s00190-015-0838-9